Published in final edited form as:
Bioconjug Chem. 2011 April 20; 22(4): 808–818. doi:10.1021/bc100478k.

A Novel Method to Label Solid Lipid Nanoparticles (SLNs) with ^{64}Cu for Positron Emission Tomography (PET) Imaging

Erica Andreozzi[1], **Jai Woong Seo**[2], **Katherine Ferrara**[2], and **Angelique Louie**[*]
[1,2] Department of Biomedical Engineering, University of California, Davis, CA 956716

Abstract

Solid lipid nanoparticles (SLNs) are sub-micron (1–1000 nm) colloidal carriers developed in the last decade as an alternative system to traditional carriers (emulsions, liposomes and polymeric nanoparticles) for intravenous applications.(1) Because of their potential as drug carriers, there is much interest in understanding the *in vivo* biodistribution of SLNs following intravenous (i.v) injection. Positron Emission Tomography (PET) is an attractive method for investigating biodistribution but requires a radiolabeled compound. In this work, we describe a method to radiolabel SLN for *in vivo* PET studies. A copper specific chelator, 6-[p-(bromoacetamido)benzyl]-1,4,8,11-tetraazacyclotetradecane-*N*,*N*′,*N*″,*N*‴-tetraacetic acid (BAT), conjugated with a synthetic lipid,(2) was incorporated into the SLN. Following incubation with $^{64}CuCl_2$ for 1 hr at 25 °C in 0.1 M NH_4OAc buffer (pH 5.5), the SLNs (~150 nm) were successfully radiolabeled with ^{64}Cu (66.5% radiolabeling yield), exhibiting >95% radiolabeled particles following purification. The ^{64}Cu-SLNs were delivered intravenously to mice and imaged with PET at 0.5, 3, 20, and 48 hr post injection. Gamma counting was utilized post imaging to confirm organ distributions. Tissue radioactivity (% injected dose/gram, %ID/g) obtained by quantitative analysis of the images suggests that the ^{64}Cu-SLNs are circulating in the bloodstream after 3 hr (blood half life ~1.4 hr), but are almost entirely cleared by 48 hr. PET and gamma counting confirm approximately 5–7 %ID/g ^{64}Cu-SLNs remaining in the liver at 48 hr post injection. Stability assays confirm that copper remains associated with the SLN over the 48 hr time period and that the biodistribution patterns observed are not from free, dissociated copper. Our results indicate that SLNs can be radiolabeled with ^{64}Cu and their biodistribution can be quantitatively evaluated by *in vivo* PET imaging and *ex vivo* gamma counting.

Keywords

solid lipid nanoparticle (SLN); Cu-64; PET; radiolabeling yield; particle stability; biodistribution

INTRODUCTION

Solid lipid nanoparticles (SLNs) have emerged as an efficient, non-toxic, and versatile colloidal drug carrier system that avoids some of the disadvantages of liposomes and polymeric nanoparticles.(1) Because SLNs are composed of physiological lipids (i.e. fatty acids, mono, di and triglycerides, phospholipids, etc.), they tend to show high compatibility and biodegradability and have lower risk of the acute and chronic toxicity that is often associated with polymeric nanoparticles.(3–4) Furthermore, because SLNs are comprised of a solid lipid core instead of an aqueous core, they offer better protection against chemical degradation to their drug cargo than liposomes, and also facilitate sustained drug release due

[*]To whom correspondence should be addressed: Prof. Angelique Y. Louie, Dept. of Biomedical Engineering, 451 East Health Sciences Drive, University of California, Davis, Davis, CA 95616, Phone: (530) 752-7134, aylouie@ucdavis.edu.

to the zero-order kinetic breakdown of the solid lipid matrix.(1, 3–4) The solid lipid matrix of the SLN core can be modified to incorporate either hydrophobic or hydrophilic cargo.(4–6) The capability of SLNs to stably carry various types of cargo-proteins(7–8) (cyclosporine(9), insulin,(10), thymopentin,(11) etc.), antibiotics (tobramycin(12)), therapeutic agents(13) (camptothecin,(14), doxorubicin(15), DNA,(16–17), siRNA,(18)), and diagnostic agents (gadolinium,(19–20) iron oxide nanoparticles,(21)) under various routes of administration (i.e. oral,(10) parenteral,(22) dermal,(23–24) ocular,(25–26) pulmonary,(27) and intravenous(28)) has generated increasing interest in their use as drug carriers.

To date, most of the studies evaluating SLNs as a drug carrier have focused on the delivery of the SLN cargo (i.e. encapsulated drug)(14, 29) to the target site without investigating the fate of the SLN carrier itself. However, with the potential for release of cargo, it is crucial to understand the biodistribution of the carrier. This is especially important in guiding the appropriate SLN modifications necessary to control drug targeting behavior in a variety of applications. The aim of this work was to radiolabel SLNs with a positron emitting radionuclide (i.e. ^{64}Cu) in order to track their biodistribution *in vivo* using positron emission tomography (PET). PET is a noninvasive, nuclear imaging technique that is capable of visualizing deep tissues with a high sensitivity of 0.02–0.10 cps/Bq (2–10%)(30) and generating a three-dimensional image of living subjects. Using mathematical reconstruction methods and correction factors, quantitative information can be extracted from the images and radioisotope concentration can be measured in a specific region of interest (ROI).(30–31) Herein, we describe a method to radiolabel SLNs with positron emitter ^{64}Cu (half life = 12.7 hr)(32) through the incorporation of a lipid-PEG-chelate (6-[p-(bromoacetamido)benzyl]-1,4,8,11-tetraazacyclotetradecane-*N*,*N*′,*N*″,*N*‴-tetraacetic acid (BAT) conjugated to a synthetic lipid)(2) into the phospholipid monolayer comprising the SLN surface (Figure 1). PET imaging was used to track the biodistribution of the SLN and followed up to 48 hr following intravenous (i.v.) administration.

EXPERIMENTAL PROCEDURES

Materials

Laboratory-grade vegetable lecithin, stearic acid, and 1-butanol were purchased from Fisher Chemical (Pittsburg, PA). Sodium taurodeoxycholate hydrate, high purity ammonium acetate (≥ 99.995%), and Sephadex® (G-25, G-50) were purchased from Sigma-Aldrich (St. Louis, MO). Bovine serum albumin was from Acros Organics, Belgium, distributed by Fisher Scientific. 5-(and-6)-carboxytetramethylrhodamine, succinimidyl ester (5(6)-TAMRA, SE) *mixed isomers* (TAMRA) (E_x = 555 nm, E_m = 580 nm) was purchased from Invitrogen Corporation (Carlsbad, CA). Formvar® Coated Copper Grids (300 Mesh) were purchased from SPI Supplies (West Chester, PA). $^{64}CuCl_2$ was purchased from Washington University (St. Louis, MO). Nanopure water (18.0 MΩ·cm) was prepared from deionized water using a Barnstead nanopure filtration unit.

Encapsulation of fluorescently labeled protein into SLN

Fluorescent labeling of BSA—Bovine serum albumin (BSA) was labeled with the fluorophore, 5(6)-carboxytetramethyl-rhodamine N-hydroxy-succimide ester (TAMRA), following the standard Invitrogen protocol for labeling proteins with amine-reactive fluorophores. First, BSA was dissolved in 0.1 M sodium bicarbonate buffer (10 mg/ml). TAMRA (10 mg/ml in Dimethyl sulfoxide) was slowly added to the BSA solution in a 2:1 molar ratio of TAMRA to BSA under continuous stirring for 1 hour at room temperature. The unlabeled TAMRA was separated from the BSA-TAMRA conjugate through a Sephadex® (G-25) packed bed column equilibrated with 0.1 M sodium bicarbonate buffer.

After separation, the BSA-TAMRA conjugate was dialyzed (50,000 MWCO) for 3 days with 0.1 M sodium citrate (pH 7.2) to remove buffer salts.(33) BSA-TAMRA was encapsulated into solid lipid nanoparticles (SLNs) using a modification of a Water/Oil/Water method.(11, 34)

Incorporation of labeled BSA into SLN: Water/Oil/Water Method—A warm W/O phase was first prepared by adding a warm aqueous solution of BSA-TAMRA (300 mg/ml) to a mixture of molten stearic acid, lecithin, and 1-butanol at 78°C (Table 1). The W/O phase was then cooled to room temperature, and a portion of this warm solid phase was added to a warm mixture of nanopure water, lecithin, sodium taurodeoxycholate, and 1-butanol at 76°C forming a W/O/W emulsion (amounts given in Table 1). The W/O/W (~0.3 ml) was then dispersed in 10 ml of cold nanopure water (1/33, v/v) at 4°C under rapid stirring, forming SLNs. The resulting SLN suspension was filtered through Millipore polyethersulfone syringe-filter units (0.22 μm pore size, Millipore) to select for particles <220 nm. Then, the SLN-BSA-TAMRA suspension (10 ml) was washed (3x) with nanopure water and concentrated (2 ml) using an Amicon ultrafiltration cell with 100,000 MWCO membrane filters (Millipore).

Characterization (size, morphology, encapsulation efficiency, toxicity) of SLN —The average size and polydispersity index (PDI) of the protein-loaded SLNs were determined with dynamic light scattering (DLS) immediately following synthesis (Nanotrac 150 particle size analyzer, Microtrac). Particle size was also measured using transmission electron microscopy (TEM) (Phillips CM-120) operating at 80keV. The SLN suspensions were diluted 10 and 20-fold and plated onto Formvar® coated copper grids (300 Mesh) to dry overnight. Images were analyzed using *ImageJ* software (National Institutes of Health) and n = 500 particles were measured to yield average particle diameter. In addition to size analysis, the zeta potential of the SLNs was measured with a NICOMP 380 ZLS (Particle Sizing System, CA).

The amount (mg) of BSA-TAMRA found in the retentate (SLN-BSA-TAMRA) and the elutant (free BSA-TAMRA) after ultrafiltration was determined by measuring the fluorescence intensity (Fluoromax) at 580 nm and used to characterize the amount of fluorescently-labeled protein encapsulated by the SLN. The % encapsulation efficiency (%EE) of the protein within the SLNs was calculated according to the following equation:

$$\%EE=[\text{BSA}-\text{TAMRA (mg) in retentate}]/[\text{BSA}-\text{TAMRA (mg) in retentate+elutant}]\times 100\%$$

Cytotoxicity Measurements—Madin-Darby canine kidney cells (MDCK), a kind gift from the Reen Wu lab (University of California, Davis), were plated onto 96 well plates at a seeding density ~1×10^3 cells per well. The cells were maintained in phenol-red free Dulbecco's Eagle minimum essential medium (DMEM), supplemented with 2 mM L-glutamine, 10% Fetal Bovine Serum (FBS), and streptomycin/penicillin (100 U/ml) at 5% CO_2 and 37°C. The medium was changed every other day until the cells reached confluency, then the cells were washed three times with phosphate buffered saline (PBS)(35) and 100 μl of a 25 mM (lipid concentration) solid lipid nanoparticle (SLN) suspension was added above the cell monolayer in each well for the experimental group, while phenol-red free DMEM was added for the control. The SLNs in this suspension were reconstituted in DMEM free of phenol-red indicator in order to prevent any interference with the cell viability fluorescence assay measurements. The cells were incubated with the SLN for 24 h (5% CO_2, 37°C) and then the medium was removed. Next, 100 μL of a LIVE/DEAD® working solution (Invitrogen) containing 1 μM calcein AM and 2 μM EthD-1 was added to each well and allowed to incubate at room temperature for 30 min. Calcein (Ex/Em ~495 nm/~515 nm) is

only retained in live cells, and cell viability was quantified by measuring the fluorescence (Ex/Em ~495 nm/~525 nm) of the cells using a microplate spectrophotometer (Safire II, Tecan Group Ltd.) The average fluorescence (Ex/Em ~495 nm/~515 nm) intensities of the cells incubated with and without SLNs (lipid concentration = 25 mM) were measured. A two-tailed *t*-test was performed to determine if there was a significant difference in viability between the cells that had been incubated with the SLNs and controls.

Radiolabeling, purification, and stability of protein-loaded SLNs

Incorporation of BAT chelator into the SLN (SLN-BAT)—Solid lipid nanoparticles (SLNs) were synthesized using the same W/O and W/O/W phase compositions as above, shown in Table 1, with the exception of adding 164.7 μg (0.062 μmol, 0.5% mol/mol ratio BAT to lipid) lipid-PEG-BAT (164.7 μl of 1 μg/μl solution) to the warm mixture of nanopure water, lecithin, sodium taurodeoxycholate, and 1-butanol before the addition of the W/O phase in the W/O/W formation. We used lipid-PEG-BAT conjugate previously synthesized by Fmoc solid phase synthesis and purified by reverse phase high performance liquid chromatography (HPLC), with the mass confirmed by matrix-assisted laser desorption/ionization (MALDI) (measured, 2662).(2) The W/O/W (~0.3 ml) was then dispersed in 10 ml of cold nanopure water (1/33, v/v) at 4°C under rapid stirring, forming SLNs. The SLNs were then filtered through Millipore polyethersulfone syringe-filter units (0.22 μm pore size, Millipore) to select for particles <220 nm and particle size was determined using DLS. Immediately after sizing, the SLN suspension (10 ml) was washed (3x) and concentrated to 200 μl using an Amicon ultrafiltration cell with 300,000 MWCO membrane filters (Millipore).

^{64}Cu Radiolabeling of SLN-BAT (^{64}Cu-SLN)—An aliquot of 0.1 M ammonium acetate. (NH_4OAc solution, pH 5.6) was added to the concentrated SLN-BAT solution to adjust the pH to 5.5. Cupric-64 chloride ($^{64}CuCl_2$) solution (4.1–5.1 mCi, 151.7–188.7 MBq in 10 mM HCl) was combined with the SLN-BAT solution, resulting in final concentration of ~10 mCi/ml and ~1.3 mCi/mg lipid. After vortexing, this solution was incubated for 1 h at room temperature. Then, EDTA solution (0.1 M, 30 μl, 1/10 v/v ratio) was added (final EDTA concentration 10 mM) to the mixture and incubated for 30 min at room temperature in order to chelate the unbound ^{64}Cu. Free ^{64}Cu-EDTA was removed from the ^{64}Cu-SLN suspension (0.3 ml) by chromatography through a G-50 Sephadex® column (GE Healthcare, NJ) eluted with 0.9% saline, and the eluted fractions (~1.0 ml) were collected in 1.5 ml centrifuge tubes. Radioactivity of the ^{64}Cu-SLN suspension before and after column purification was measured with a Fluke Biomedical Dose calibrator (34–162 CAL/RAD MARK IV, Cleveland, OH). The radiolabeling yield (%) for the SLNs was determined by dividing the radioactivity of the largest fraction by the sum of all the fractions (total activity) and multiplying by 100. Thin layer chromatography (TLC) of the purified ^{64}Cu-SLNs was run on aluminum-backed silica gel sheets (silica gel 60 F_{254}, EMD, NJ), developed with methanol/ammonium acetate (10%) (50/50, v/v), and the radio TLC was recorded by a radio-TLC Imaging Scanner (Bioscan, NW).

Stability of ^{64}Cu-SLNs—^{64}Cu-labeled SLNs were incubated in calf bovine serum (100%, pH 7.4) and saline solutions with varying pH (5.5, 4.0, and 2.0) for up to 48 hr in order to assess the stability of the complexed copper before and after administration in mice. An aliquot (100 μl) was removed at each time point (0.5, 3, 20, and 48 hr) and measured for initial activity (before purification) using a dose calibrator. The aliquots were incubated for 10 minutes with 10 μl (1/10, v/v) EDTA (0.1 M in water) and centrifuged through filter tubes (Millipore, molecular weight cutoff [MWCO] = 10,000, Billerica, MA) at 14,500 rpm for 30 min to separate dissociated ^{64}Cu-EDTA in solution from the labeled SLNs on the filter. The activity remaining on the filter post purification was measured and divided by the

initial activity to calculate the percentage (%) of label remaining on the SLNs. Comparisons between values were determined using the least squares means *t*-test, and differences observed were considered significant when $p < 0.01$. For further confirmation of stability, radio TLC was performed on aliquots of ^{64}Cu-SLNs incubated with serum for 24 and 48 hr. EDTA was used to chelate unbound ^{64}Cu in both the centrifugation purification and radio TLC measurements.

In vivo studies: Biodistribution & Pharmacokinetics of ^{64}Cu-SLN using PET imaging and gamma counting

All animal studies were conducted under a protocol approved by the University of California, Davis Animal Use and Care Committee. A total of 3 mice (female, 39.71 ± 3.11 g, Charles River, MA) were examined over the course of this study. Mice were initially anesthetized with 3.0% isofluorane, then maintained at 2.0%–2.5% isoflurane, and catheterized to ensure proper tail vein injection. Injections (280–320 μl) of ^{64}Cu-SLN (409.01 ± 43.11 μCi, 15.1 ± 1.6 MBq, 9.9 ± 1.6 mg) in 0.9% saline were administered via tail vein injection, yielding a lipid dose of 0.27 ± 0.04 mg/g animal and 38.36 ± 7.16 μCi/mg lipid (1.4± 0.3 MBq/mg lipid). Static PET scans (0.25, 1.0, 0.75, and 1.0 hr duration scans) were acquired for each animal (anesthetized with 1.5% isoflurane maintenance dose) at 0.5, 3.0, 20, and 48-hr post injection using the MicroPETII scanner.(36) The MicroPETII consists of 17 640 LSO crystals each measuring 0.975 × 0.975 × 12.5 mm^3, which are arranged in 42 contiguous rings, with 420 crystals per ring. The scanner has an axial field of view (FOV) of 4.9 cm and a transaxial FOV of 8.5 cm.(37) The limited transaxial FOV of ~8.5 cm only enabled signal acquisition from the top of the head to the liver region. Therefore, signal from organs below the liver (i.e. kidney, bladder, etc.) was not included in the images. The reconstructed spatial resolution is ~1 mm with an absolute system sensitivity of 2.26%.(36) Static scans yield a single image that represents the average intensities for a given acquisition time.

The static PET scans were reconstructed with a maximum a posteriori (MAP) algorithm and used to obtain quantitative activity levels in each organ of interest as a function of time. Tissue radioactivity was determined using the mean activity value given by the ASIPro Virtual Machine software (CTI Molecular Imaging) from defined regions of interest (ROI) within these MAP files. All values for ROI were decay corrected to the zero hour time point for comparison, and the percent injected dose (%ID) was determined by dividing the corrected ROI value for a given organ by the injected dose and multiplying by 100. A time activity curve (TAC) for blood was generated by drawing 0.03 cm^2 ROIs within the heart (~5 slices) for all time points (0.5, 3, 20, 48 hr) and expressing the mean measured activity as the percentage of injected dose per cubic centimeter (%ID/cc). A monoexponential curve was fit to the data series and used to estimate the blood half-life for the ^{64}Cu-SLNs.

After the 48 hr PET scans, the mice were euthanized by administration of sodium pentobarbital (150 mg/kg) and perfused with 60 ml of 0.9% saline. Organs of interest were harvested and weighed and radioactivity was measured using a Wallac Wizard Automatic Gamma Counter Model 1470 (Perkin Elmer, Waltham, MA) at 52–55 hr post i.v. injection. One way analysis of variance (ANOVA) was conducted in Prism (GraphPad software Inc. San Diego, CA) and used to assess the significance of organ biodistribution.

RESULTS & DISCUSSION

Preparation and characterization (size, morphology, charge, toxicity) of protein-loaded SLNs

Because the size and the charge of nanoparticles are known to significantly influence their fate *in vivo*, it was important to measure these particle properties for SLNs. Using dynamic light scattering (DLS), the mean hydrodynamic diameter of the SLNs was determined to be 145 ± 0.07 nm (Figure 2a). From the TEM images in Figure 2b, we observe that the SLNs exist as a uniform, monodisperse population of spherical particles with a diameter of 86 ± 0.6 nm (n = 500 particles, *ImageJ*). We believe that the difference in SLN diameter measured from DLS (~150 nm) compared to TEM (~90 nm) is due to the inability of TEM detect the hydration shell that surrounds the phospholipid monolayer of the SLN. By either measurement, the SLNs fall into the 20–200 nm size range reported for particles capable of avoiding rapid clearance through the kidneys,(6) thus making them attractive carriers for *in vivo* drug delivery.

To assess the stability of the SLN in suspension, we measured their zeta potential. A high zeta potential will confer stability (i.e. the solution or dispersion will resist aggregation) with the dividing line between stable and unstable suspensions generally considered to be at ± 30 mV, and with maximum electrostatic stabilization reached at around ±60 mV.(38) The SLNs were measured to have a zeta potential of −36 mV, indicating an electrically stable, anionic particle solution. Previous studies show that negatively charged particles ≥ −30 mV have good stability and could be optimal for drug delivery.(39–40) Aside from governing particle stability, zeta potential also influences particle recognition by the reticuloendothelial system (RES). In a previous study by Manjunath et al, highly negatively charged (−35.1 ± 0.5 mV) SLNs exhibited higher effective bioavailability (60.4%) of the encapsulated drug than less negatively charged particles (−18.2 ± 0.3 mV) SLNs (44.4%).(29) This is consistent with other studies showing that liposomes formed with negatively charged phospholipids maintained prolonged circulation time in mice.(41)

In order to provide an optical handle to track SLN during purification and characterization, we synthesized SLNs containing bovine serum albumin (BSA) labeled with the fluorophore, TAMRA. The encapsulation efficiency (EE, %) of BSA-TAMRA within SLNs was approximately 86.9 ± 5.3%, which is relatively high in comparison to other reported hydrophilic cargoes.(3–5, 8, 42) For example, the maximum EE for the hydrophilic drug Zidovudine (an anti-human immunodeficiency viral agent) in SLNs composed of stearic acid was 27%.(43) Because lipophilic agents have high solubility in the lipid microemulsion preceding SLN formation, SLNs are more efficiently loaded with lipophilic drugs. Entrapment of hydrophilic drugs inside the hydrophobic matrix of SLNs is a bit more challenging because the drug has a tendency to partition into the water phase during the fabrication process.(43) SLNs thus incorporate hydrophilic drugs at lower encapsulation efficiencies.(7, 42, 44–46) Zidovudine(43), Atazanavir(46), thymocratin(47), insulin(10), diminazene(48), and thymopentin(11) are examples of hydrophilic drugs that have been successfully incorporated into SLNs. Interestingly, Singh et al found that fatty acids (i.e. stearic acid) were superior to triglycerides to enhance entrapment efficiency.(49) This is consistent with our observations of high EE for BSA-TAMRA (hydrophilic protein) encapsulated in our SLNs, whose primary lipid was stearic acid. Furthermore, encapsulation of the hydrophilic HIV protease inhibitor, Atazanavir, into SLNs of similar size (~167 nm) and composition (stearic acid) to our SLNs resulted in a similar EE (~90%).(46) These results suggest that using stearic acid as the primary lipid component of our SLNs is favorable for achieving high EE of hydrophilic cargo.

Toxicity of the SLNs was assessed *in vitro*. Incubation (24 hr) of SLNs at a lipid concentration of 25 mM with MDCK cells (data not shown) showed no statistical difference (p-value = 0.51) in viability compared to controls. The 25 mM lipid concentration that was tested *in vitro* was ~2.5 times larger than the concentration of the injected dose to be used for *in vivo* studies. The lipid (molecular weight ~500 g/mol) dose to each mouse was approximately 10 mg, yielding a circulating lipid dose of ~10 mM, assuming total mouse blood volume ~2 ml. These results are consistent with previous investigations of stearic acid based SLNs that found them to be non-toxic to human promyelocytic leukemia (HL60) and human breast adenocarcinoma (MCF-7) cell lines.(42, 50) In comparison to SLNs, FDA-approved polyester nanoparticles, i.e. poly(lactic-co-glycolic acid) (PLGA), polylactic acid (PLA), etc., were 10- 20-fold more toxic to human granulocytes.(9, 42) The low cytotoxicty of SLNs makes them very attractive for drug delivery, especially to highly sensitive organs like the brain.(42) Also, the ability to load drugs into SLNs with a high encapsulation efficiency (EE), such as 86.9 ± 5.3% observed with our system, further reduces the potential for cytotoxicity by reducing the dose of particles required to achieve a pharmacological effect. Overall, these *in vitro* cytotoxicity studies suggest that SLNs are nontoxic and that they can be used for *in vivo* animal imaging studies.

Preparation and Characterization (radiolabeling, purification, stability) of ^{64}Cu-SLNs

Because the goal of this study was to track the biodistribution of the SLN carrier and not the cargo, we used a surface chelation method to radiolabel the SLNs with ^{64}Cu. This chelation method required the incorporation of a lipid-PEG-chelate conjugate into the SLN so that the chelator remains accessible at the surface for ^{64}Cu chelation. We previously showed that liposomes could be radiolabeled after incorporation of this lipid-PEG-chelate conjugate into the liposome bilayer.(2)

High SLN radiolabeling yield (%)—A ^{64}Cu-specific chelator, 6-[p-(bromoacetamido)benzyl]-1,4,8,11-tetraazacyclotetradecane-N,N′,N″,N‴-tetraacetic acid (BAT), conjugated to stearic acid (lipid-PEG-BAT) has been previously synthesized and used to radiolabel liposomes with ^{64}Cu,(2) and we hypothesized that this lipid-PEG-BAT molecule could function similarly to radiolabel our SLNs. We anticipated that the lipid portion of the lipid-PEG-BAT molecule would be incorporated into the solid lipid core, the PEG would be associated at the level of the lecithin head-groups, and the BAT would remain accessible on the surface. The elution profiles of radiolabeled SLNs following column purification are shown in Figure 3a, with fraction 2 representing the purified ^{64}Cu-SLN population. Fraction 2 was analyzed by radio-TLC as shown in Figure 3b. The TLC peak (green bar, 96.7%) represents ^{64}Cu-SLNs, which remain at the baseline. The negligible amount (2.94%) of free ^{64}Cu in the purified ^{64}Cu-SLN suspension confirms >95% radiolabeled particles. The radiolabeling yield (%) of SLNs was approximately 66.8%.

High stability of radiolabeled SLNs—A stability assay was performed in order to confirm that Cu-64 remains associated with the SLN over the 48 hr time period and that the biodistribution patterns observed are not from free, dissociated Cu-64. Figure 4 shows that over time (0.5, 3, 20, and 48 hr), the SLNs in saline and serum do not lose radiolabel. The saline solution is a control to test the stability of the particles in solution before intravenous (i.v.) administration, while the serum solution mimics blood circulation. Because the molecular weight of the lipid-PEG-BAT is less than the 10,000 MWCO of the centrifugal filters used for purification, both dissociated free copper and dissociated lipid-PEG-BAT molecules are removed during centrifugation purification, while nanoparticles are retained in the filtrate. Radio TLC experiments (Fig. 5) confirm that no peak corresponding to free ^{64}Cu (~85 mm, Retention factor (R_f) = 0.66) was observed for filtrates after 24 and 48hr incubation in serum, verifying the stability of these radiolabeled particles in the bloodstream

up to 48 hr. Overall, the results of this stability assay confirm that there is no significant loss ($p < 0.01$) of free copper or free lipid-PEG-BAT (chelated with Cu-64) from the SLNs in saline or plasma. Although the SLNs were quite stable in serum and in saline at pH 5.5, they showed a significant loss (p value > 0.01) of label over time when incubated in pH 2 and pH 4. Radio TLC was performed on the supernatants collected after centrifugation filtration of the SLNs incubated with saline (pH 2) and saline (pH 4) at 3 and 20 hr. It is clear from these TLC plots (Fig 6) that saline (pH 2) and saline (pH 4) supernatant yield single peaks corresponding to ^{64}Cu (~85 mm, $R_f = 0.66$). This confirms that the loss of radiolabel for saline (pH 2) and saline (pH 4) observed in Figure 4 was due to free ^{64}Cu dissociating from the particle in these extreme conditions. Saline at pH 2 and saline at pH 4 were used to mimic the acidic conditions of the stomach and lysosomes, both environments the SLNs are not likely to encounter. Therefore, the observed ^{64}Cu dissociation at these conditions is not of significant concern.

Preliminary biodistribution & pharmacokinetics of ^{64}Cu-SLN *In vivo* using PET imaging and gamma counting

Radiolabeling SLNs with ^{64}Cu facilitates the use of positron emission tomography (PET) for the investigation of SLN biodistribution *in vivo*. Imaging seldom has been used to describe the biodistribution of SLNs following i.v. administration. Instead, most researchers label SLNs with a gamma-emitting radioisotope and report biodistribution by gamma counting organs. For example, gamma counting methods have been used to describe full-body biodistribution of Technetium-99m (^{99m}Tc)-labeled SLNs following endotracheal administration to mice(51) and Iodine-125 (^{125}I)-labeled SLNs following intravenous injection to rats.(28) Our results confirm a method to radiolabel solid lipid nanoparticles with ^{64}Cu through the incorporation of a lipid-PEG-BAT chelating molecule into SLNs carrying a cargo of fluorescently labeled hydrophilic protein (bovine serum albumin).

Preliminary biodistribution and blood clearance of the radiolabeled SLNs (^{64}Cu-SLNs) was assessed in the mouse model. From the biodistribution plot (Figure 7) obtained by gamma counting organs at 52–55 hr post i.v. injection, we observe that the liver radioactivity (6.6 ± 0.7 %ID/g) was significantly higher ($p < 0.01$) than all other organs, including heart (1.1 ± 0.4 %ID/g), lung (1.2 ± 0.5 %ID/g), gastrointestinal (GI) tract (1.7 ± 0.9 %ID/g), right (2.2 ± 0.2%ID/g) and left (1.7 ± 1.1%ID/g) kidneys, spleen (2.9 ± 1.1 %ID/g) and brain (0.03 ± 0.01%ID/g). This organ biodistribution obtained from gamma counting organs was compared with the *in vivo* biodistribution obtained from PET imaging. Figure 8a–d displays the biodistribution of ^{64}Cu-SLNs in mice from representative coronal PET images at 0.5,3, 20, and 48 hr post i.v. injection. There was obvious radioactivity in the carotids (C) and the heart (H), at 0.5 hr and 3 hr post injection (Figure 8a and b) indicating continuing circulation of the ^{64}Cu-SLNs; this signal disappeared by 20 hr post injection (Figure 8c), indicating that the ^{64}Cu-SLNs had primarily cleared the bloodstream. Figure 8a and 8b also show high liver (L) and spleen (S) activity, indicating that the ^{64}Cu-SLNs were cleared through the reticuloendothelial system (RES) by 0.5 hr and 3 hr post injection. By 20 hr post injection (Figure 5c), there was faint activity in the spleen, but more prominent was the activity in the intestines (I) and the liver (L). Verkade et. al. showed that liposome-associated phosphatidylcholine is predominantly degraded by the liver, and that these degradation products are partially secreted into bile. Thus, the radioactivity we observe in the intestines is hypothesized to result from the liver slowly breaking down the SLNs and releasing radioactivity through the bile duct.(52) This is consistent with previous studies from Seo et. al. showing radioactivity accumulation in the intestines following i.v. administration of radiolabeled liposomes in mice.(2) Only liver activity remains visible at 48 hr post injection (Figure 8d), suggesting that ^{64}Cu-SLNs were primarily cleared through the RES by this time. Radioactivity in the liver (L) decreased over time as shown in Figure 6e (25.4 ± 0.9,

22.1 ± 4.0, 11.9 ± 0.9, and 5.6 ± 1.3 %ID/g at 0.5, 3, 20, and 48 hr, respectively), validating that SLNs do not remain in liver long-term.

The liver activity at 52–55 hr measured by gamma counting (6.6 ± 0.7 %ID/g) was consistent with the liver activity measured by PET quantification (Figure 8e), which showed an average of 5.7 ± 1.1%ID/g at 48 hr. The heart activity was also consistent between the two methodologies of quantization yielding values of 0.9 ± 0.1%ID/g with PET and 1.1 ± 0.4 %ID/g with gamma counting. Nevertheless, the low activity of the other organs (lungs, GI, right kidney, left kidney, spleen, and brain) at 48 hr results in the inability for the microPETII to appropriately detect their organ boundaries; at earlier time points the activity is high enough to avoid this issue. Therefore, the use of a more sensitive (3x) PET scanner (absolute system sensitivity ~7%), such as the F120 produced by Siemens Medical Solutions, Inc. will enable one to appropriately define organ boundaries at the later time points (i.e. 48 hr) in future studies.

Blood clearance was assessed by monitoring signal from the heart over time. The time activity curve (TAC) of blood in Figure 9 showed that ^{64}Cu-SLNs were still circulating in the bloodstream after 3 hr, but were almost entirely cleared from the bloodstream by 48 hr. The monoexponential curve was fit to the data, yielding a correlation coefficient of 0.99. The blood half-life for the ^{64}Cu-SLNs was estimated to be approximately 1.4 hr. This is very different behavior from free ^{64}Cu or free ^{64}Cu radiolabeled lipid-PEG-BAT that result in blood half lives ~5–10 min and are known to clear almost entirely from the bloodstream at 15 min post i.v. injection.(2) The 1.38 ± 0.12 hr blood half life of our ^{64}Cu-SLNs was also much longer than that of most polymeric nanoparticles, which are reported to have blood lives of only a few minutes. For example, polysorbate 80 (P80) coated poly(α-butyl cyanoacrylate) (PBCA) nanoparticles loaded with ^{125}I radiolabeled quinoline derivatives and delivered to mice by intravenous (i.v.) injection were almost entirely cleared after 1 hr, with a blood half-life of ~5 min.(53) Similarly, P80-coated poly(lactic-co-glycolic acid) (PLGA) nanoparticles labeled with ^{99m}Tc were cleared very rapidly from the blood after i.v. injection in mice, with 1.28 ± 0.07%ID/g remaining at 1 hr post injection and a blood-half life of only a few minutes.(54) Overall, the RES-mediated clearance of the SLNs from the bloodstream can be reduced further by coating the SLNs with a hydrophillic or flexible polymer and/or surfactant such as polyethylene glycol (PEG) or polysorbate.(55) Coating with PEG has been shown to improve the pharmacokinetic profile of particles by reducing opsonization, phagocytosis, and clearance by the liver and RES.(55) We will investigate the influence of various hydrophilic coatings in order to reduce SLN clearance by the RES and prolong their circulation time in the blood stream. This will facilitate the possibility of longer imaging studies to assess SLNs biodistribution *in vivo*.

Because of their lipophilic nature, most interest in SLNs involves their use as carriers for drug delivery to the brain.(3, 6, 42, 55–56) The adsorption of a plasma protein, ApoE, onto the nanoparticles surface is thought to facilitate SLN uptake into the brain through the low density lipoprotein (LDL) receptors on the brain endothelial cells lining the blood brain barrier (BBB). From a close examination of the brain distribution (Figure 5), we observe approximately 0.03 ± 0.03 %ID/g of activity at 52–55 hrs post injection. This small amount of SLNs delivered to the brain could be enhanced through surface modifications, such as coating with P80.(53) P80 remains to be the most successful “stealth” coating for delivering therapeutic agents into the brain,(39, 42, 57–60) reporting values as high 0.52 %ID/g in the brain.(61) In a recent study, P80 coating of SLNs containing riluzole facilitated a significantly higher dose of riluzole to the brain in comparison to free riluzole alone.(62) Since P80 coating has also demonstrated the ability to enhance BBB transport,(63) we will coat radiolabeled SLNs with P80 and use PET to investigate the ability for SLNs to target the brain *in vivo*.

CONCLUSION

Solid lipid nanoparticles (SLNs) are a versatile colloidal drug carrier system that combines the advantages of both liposomes and polymeric nanoparticles. Because of the potential for SLN to facilitate controlled drug delivery to a target tissue, there is much interest in understanding their *in vivo* biodistribution following intravenous (i.v) injection. By incorporating a lipid-PEG-BAT chelator into the SLN monolayer, we have developed a method to radiolabel SLNs with ^{64}Cu for noninvasive mapping of biodistribution *in vivo* using PET. Preliminary *in vivo* biodistribution of these SLNs (^{64}Cu-SLNs) was evaluated in mice up to 48 hr post i.v. injection using PET, and these values were then compared to *ex vivo* biodistribution from gamma counting of organs. The blood half-life for the ^{64}Cu-SLNs was ~1.4 hr, which is longer than typical polymeric nanoparticles of similar size. Gamma counting confirmed significant activity in the liver at 48 hr post i.v. injection. Coating SLNs with hydrophilic polymers such as PEG will be investigated in the future to reduce SLN clearance by the RES (kidneys, liver, and spleen) and increase the blood half-life. Longer blood circulation times will further enhance the appeal of SLNs as drug carriers, and the ability to radiolabel these SLNs for noninvasive assessment of biodistribution *in vivo* using PET will accelerate their development in the field of drug delivery, especially those drugs targeted to the brain.

Acknowledgments

Imaging was performed at the Center for Molecular and Genomic Imaging, University of California, Davis. We would like to acknowledge Jennifer Fung and Michelle Connell for their assistance with the animal imaging. We would also like to thank Dr. Reen Wu (University of California, Davis) for his donation of a Madin-Darby canine kidney (MDCK) cell line. The authors wish to acknowledge the support of the National Institutes of Health/NIBIB EB000993-06, NIH R01CA103828 and NIHT32 EB003827.

LITERATURE CITED

1. Rai S, Paliwal R, Gupta PN, Khatri K, Goyal AK, Vaidya B, Vyas SP. Solid lipid nanoparticles (SLNs) as a rising tool in drug delivery science: One step up in nanotechnology. Curr Nanosci. 2008; 4:30–44.
2. Seo JW, Zhang H, Kukis DL, Meares CF, Ferrara KW. A Novel Method to Label Preformed Liposomes with (CU)-C-64 for Positron Emission Tomography (PET) Imaging. Bioconjugate Chem. 2008; 19:2577–2584.
3. Mukherjee S, Ray S, Thakur RS. Solid Lipid Nanoparticles: A Modern Formulation Approach in Drug Delivery System. Indian J Pharm Sci. 2009; 71:349–358. [PubMed: 20502539]
4. Martins S, Sarmento B, Ferreira DC, Souto EB. Lipid-based colloidal carriers for peptide and protein delivery - liposomes versus lipid nanoparticles. Int J Nanomed. 2007; 2:595–607.
5. Gasco MR. Lipid nanoparticles: perspectives and challenges. Advanced Drug Delivery Reviews. 2007; 59:377–378. [PubMed: 17582649]
6. Mehnert W, Mäder K. Solid lipid nanoparticles: Production, characterization and applications. Advanced Drug Delivery Reviews. 2001; 47:165–196. [PubMed: 11311991]
7. Souto EB, Almeida AJ. Solid lipid nanoparticles as a drug delivery system for peptides and proteins. Advanded Drug Delivery Reviews. 2007; 59:491–504.
8. Lee JH, Il Ahn S, Park JH, Kim YT, Khang G, Rhee JM, Lee HB. Solid lipid nanoparticles as a drug delivery system for peptides and proteins. Tissue Eng Regen Med. 2008; 5:215–228.
9. Müller RH, Runge SA, Ravelli V, Thünemann AF, Mehnert W, Souto EB. Cyclosporine-loaded solid lipid nanoparticles (SLN®): Drug-lipid physicochemical interactions and characterization of drug incorporation. Eur J Pharm Biopharm. 2008; 68:535–544. [PubMed: 17804210]
10. Sarmento B, Martins S, Ferreira D, Souto EB. Oral insulin delivery by means of solid lipid nanoparticles. Int J Nanomed. 2007; 2:743–749.

11. Morel S, Ugazio E, Cavalli R, Gasco MR. Thymopentin in solid lipid nanoparticles, International Journal of Pharmaceutics. Int J Pharm. 1996; 132:259–261.
12. Cavalli R, Zara GP, Caputo O, Bargoni A, Fundarò A, Gasco MR. Transmucosal transport of tobramycin incorporated in SLN after duodenal administration to rats. Part I--A pharmacokinetic study. Pharmacological Research. 2000; 42:541–545. [PubMed: 11058406]
13. Wong HL, Bendayan R, Rauth AM, Li Y, Wu XY. Chemotherapy with anticancer drugs encapsulated in solid lipid nanoparticles. Advanced Drug Delivery Reviews. 2007; 59:491–504. [PubMed: 17532091]
14. Yang SC, Lu LF, Cai Y, Zhu JB, Liang BW, Yang CZ. Body distribution in mice of intravenously injected camptothecin solid lipid nanoparticles and targeting effect on brain. Journal of Controlled Release. 1999; 59:299–307. [PubMed: 10332062]
15. Fundaro A, Cavalli R, Bargoni A, Vighetto D, Zara GP, Gasco MR. Non-stealth and stealth solid lipid nanoparticles (SLN) carrying doxorubicin: Pharmacokinetics and tissue distribution after i.v. administration to rats. Pharmacological Research. 2000; 42:337–343. [PubMed: 10987994]
16. Yu WY, Liu CX, Liu Y, Zhang N, Xu WF. Mannan-Modified Solid Lipid Nanoparticles for Targeted Gene Delivery to Alveolar Macrophages. Pharm Res. 2010; 27:1584–1596. [PubMed: 20422265]
17. Pedersen N, Hansen S, Heydenreich AV, Kristensen HG, Poulsen HS. Solid lipid nanoparticles can effectively bind DNA, streptavidin and biotinylated ligands. Eur J Pharm Biopharm. 2006; 62:155–162. [PubMed: 16290122]
18. Kim HR, Kim IK, Bae KH, Lee SH, Lee Y, Park TG. Cationic solid lipid nanoparticles reconstituted from low density lipoprotein components for delivery of siRNA. Mol Pharm. 2008; 5:622–631. [PubMed: 18461969]
19. Oyewumi MO, Mumper RJ. Gadolinium-loaded nanoparticles engineered from microemulsion templates. Drug Dev Ind Pharm. 2002; 28:317–328. [PubMed: 12026224]
20. Morel S, Terreno E, Ugazio E, Aime S, Gasco MR. NMR relaxometric investigations of solid lipid nanoparticles (SLN) containing gadolinium (III) complexes. Eur J Pharm Biopharm. 1998; 45:157–163. [PubMed: 9704912]
21. Peira E, Marzola P, Podio V, Aime S, Sbarbati A, Gasco MR. In vitro and in vivo study of solid lipid nanoparticles loaded with superparamagnetic iron oxide. Journal of Drug Targeting. 2003; 11
22. Joshi MD, Müller RH. Lipid nanoparticles for parenteral delivery of actives. Eur J Pharm Biopharm. 2009; 71:161–172. [PubMed: 18824097]
23. Fang JY, Fang CL, Liu CH, Su YH. Lipid nanoparticles as vehicles for topical psoralen delivery: Solid lipid nanoparticles (SLN) versus nanostructured lipid carriers (NLC). Eur J Pharm Biopharm. 2008; 70:633–640. [PubMed: 18577447]
24. Jain SK, Chourasia MK, Masuriha R, Soni V, Jain A, Jain NK, Gupta Y. Solid lipid nanoparticles bearing flurbiprofen for transdermal delivery. Drug Deliv. 2005; 12:207–215. [PubMed: 16036715]
25. Kalam MA, Sultana Y, Ali A, Aqil M, Mishra AK, Chuttani K. Preparation, characterization, and evaluation of gatifloxacin loaded solid lipid nanoparticles as colloidal ocular drug delivery system. Journal of Drug Targeting. 2010; 18:191–204. [PubMed: 19839712]
26. Basaran E, Demirel M, Sirmagul B, Yazan Y. Cyclosporine-A incorporated cationic solid lipid nanoparticles for ocular delivery. J Microencapsul. 2010; 27:37–47. [PubMed: 19545226]
27. Nassimi M, Schleh C, Lauenstein HD, Hussein R, Hoymann HG, Koch W, Pohlmann G, Krug N, Sewald K, Rittinghausen S, Braun A, Muller-Goymann C. A toxicological evaluation of inhaled solid lipid nanoparticles used as a potential drug delivery system for the lung. Eur J Pharm Biopharm. 2010; 75:107–116. [PubMed: 20206256]
28. Weyhers H, Lobenberg R, Mehnert W, Souto EB, Kreuter J, Muller RH. In vivo distribution of I-125-radiolabelled solid lipid nanoparticles. Pharm Ind. 2006; 68:889–894.
29. Manjunath K, Venkateswarlu V. Pharmacokinetics, tissue distribution and bioavailability of clozapine solid lipid nanoparticles after intravenous and intraduodenal administration. Journal of Controlled Release. 2005; 107:215–228. [PubMed: 16014318]
30. Cherry SR. Fundamentals of positron emission tomography and applications in preclinical drug development. J Clin Pharmacol. 2001; 41:482–491. [PubMed: 11361044]

31. Cherry, SR.; Sorenson, JA.; Phelps, ME. Physics in Nuclear Medicine. 3. Saunders; Philadelphia, PA: 2003. Counting systems and the gamma camera.
32. Liu S. The role of coordination chemistry in the development of target-specific radiopharmaceuticals. Chem Soc Rev. 2004; 33:445–461. [PubMed: 15354226]
33. Gustafsson B, Youens S, Louie AY. Development of contrast agents targeted to macrophage scavenger receptors for MRI of vascular inflammation. Bioconjugate Chem. 2006; 17:538–547.
34. Silvia M, Gasco MR, Cavalli R. Incorporation in lipospheres of [D-Trp-6]LHRH. Int J Pharm. 1994:105.
35. Wang Q, Rager JD, Weinstein K, Kardos PS, Dobson GL, Li JB, Hidalgo IJ. Evaluation of the MDR-MDCK cell line as a permeability screen for the blood-brain barrier. Int J Pharm. 2005; 288:349–359. [PubMed: 15620875]
36. Tai YC, Chatziioannou AF, Yang Y, Silverman RW, Meadors K, Siegel S, Newport DF, Stickel JR, Cherry SR. MicroPET II: design, development and initial performance of an improved microPET scanner for small-animal imaging. Phys Med Biol. 2003; 48:1519–37. [PubMed: 12817935]
37. Yang YF, Tai YC, Siegel S, Newport DF, Bai B, Li QZ, Leahy RM, Cherry SR. Optimization and performance evaluation of the microPET II scanner for in vivo small-animal imaging. Physics in Medicine and Biology. 2004; 49:2527–2545. [PubMed: 15272672]
38. Heurtault B, Saulnier P, Pech B, Venier-Julienne M, Proust J, Phan-Tan-Luu R, Benoît J. The influence of lipid nanocapsule composition on their size distribution. European Journal of Pharmaceutical Sciences. 2003; 18:55–61. [PubMed: 12554073]
39. Ringe K, Waltz C. Nanoparticulate Drug Delivery to the Brain. Encyclopedia of Nanoscience and Nanotechnology. 2004; 7:91–104.
40. Chen DB, Yang TZ, Lu WL, Zhang Q. In vitro and in vivo study of two types of long-circulating solid lipid nanoparticles containing paclitaxel. Chem Pharm Bull. 2001; 49:1444–1447. [PubMed: 11724235]
41. Park YS, Maruyama K, Huang L. Some negatively charged phospholipid derivatives prolong the liposome circulation in vivo. Biochimica Et Biophysica Acta. 1992; 1108:257–260. [PubMed: 1637850]
42. Blasi P, Giovagnoli S, Schoubben A, Ricci M, Rossi C. Solid lipid nanoparticles for targeted brain drug delivery. Advanced Drug Delivery Reviews. 2007; 59:454–477. [PubMed: 17570559]
43. Singh S, Dobhal AK, Jain A, Pandit JK, Chakraborty S. Formulation and Evaluation of Solid Lipid Nanoparticles of a Water Soluble Drug: Zidovudine. Chem Pharm Bull. 2010; 58:650–655. [PubMed: 20460791]
44. Ugazio E, Cavalli R, Gasco MR. Incorporation of cyclosporin A in solid lipid nanoparticles (SLN). Int J Pharm. 2002; 241:341–344. [PubMed: 12100861]
45. García-Fuentes M, Torres D, Alonso MJ. Design of lipid nanoparticles for the oral delivery of hydrophilic macromolecules. Colloids and Surfaces B: Biointerfaces. 2003; 27:159–168.
46. Chattopadhyay N, Zastre J, Wong HL, Wu XY, Bendayan R. Solid Lipid Nanoparticles Enhance the Delivery of the HIV Protease Inhibitor Atazanavir, by a Human Brain Endothelial Cell Line. Pharm Res. 2008:25. [PubMed: 18161013]
47. Reithmeier H, Herrmann J, Gopferich A. Lipid microparticles as a parenteral controlled release device for peptides. Journal of Controlled Release. 2001; 73:339–350. [PubMed: 11516510]
48. Olbrich C, Gessner A, Schroder W, Kayser O, Muller RH. Lipid-drug conjugate nanoparticles of the hydrophilic drug diminazene - cytotoxicity testing and mouse serum adsorption. Journal of Controlled Release. 2004; 96:425–435. [PubMed: 15120899]
49. Li Z, Li XW, Zheng LQ, Lin XH, Geng F, Yu L. Bovine Serum Albumin Loaded Solid Lipid Nanoparticles Prepared by Double Emulsion Method. Chem Res Chin Univ. 2010; 26:136–141.
50. Miglietta A, Cavalli R, Bocca C, Gabriel L, Gasco MR. Cellular uptake and cytotoxicity of solid lipid nanospheres (SLN) incorporating doxorubicin or paclitaxel. Int J Pharm. 2000; 210:61–67. [PubMed: 11163988]
51. Videira MA, Gano L, Santos C, Neves M, Almeida AJ. Lymphatic uptake of lipid nanoparticles following endotracheal administration. J Microencapsul. 2006; 23:855–862. [PubMed: 17390627]

52. Verkade HJ, Derksen JTP, Gerding A, Scherphof GL, Vonk RJ, Kuipers F. Differential hepatic processing and biliary-secretion of headgroup and acyl chains of liposomal phosphatidylcholines. Biochem J. 1991; 275:139–144. [PubMed: 2018469]

53. Roney C, Kulkarni P, Arora V, Antich P, Bonte F, Wu AM, Mallikarjuana NN, Manohar S, Liang HF, Kulkarni AR, Sung HW, Sairam M, Aminabhavi TM. Targeted nanoparticles for drug delivery through the blood-brain barrier for Alzheimer's disease. Journal of Controlled Release. 2005; 108:193–214. [PubMed: 16246446]

54. Halder KK, Mandal B, Debnath MC, Bera H, Ghosh LK, Gupta BK. Chloramphenicol-incorporated poly lactide-co-glycolide (PLGA) nanoparticles: Formulation, characterization, technetium-99m labeling and biodistribution studies. Journal of Drug Targeting. 2008; 16:311–320. [PubMed: 18446610]

55. Kaur IP, Bhandarib R, Bhandarib S, Kakkara V. Potential of solid lipid nanoparticles in brain targeting. Journal of Controlled Drug Release. 2008:127.

56. Kreuter J, Shamenkov D, Petrov V, Ramge P, Cychutek K, Koch-Brandt C, Alyautdin R. Apolipoprotein-mediated transport of nanoparticle-bound drugs across the blood-brain barrier. Journal of Drug Targeting. 2002; 10:317–325. [PubMed: 12164380]

57. Ramge P, Unger RE, Oltrogge JB, Zenker D, Begley D, Von Briesen H, Kreuter J. P80 coating enhances uptake of polybutylcyanoacrylate (PBCA)-nanoparticles by human and bovine primary brain capillary endothelial cells. European Jouranl of Neuroscience. 2000; 12:1931–1940.

58. Goppert TM, Muller RH. Protein adsorption patterns on poloxamer- and poloxamine-stabilized solid lipid nanoparticles (SLN). European Journal of Pharmaceutics and Biopharmaceutics. 2005; 60:361–372. [PubMed: 15996577]

59. Reimold I, Domke D, Bender J, Seyfried CA, Radunz HE, Fricker G. Delivery of nanoparticles to the brain detected by fluorescence microscopy. European Journal of Pharmaceutics and Biopharmaceutics. 2008; 70:627–632. [PubMed: 18577452]

60. You J, Wan F, Cui F, Sun Y, Du Y, Hu F. Preparation and characteristic of vinorelbine bitartrate-loaded solid lipid nanoparticles. International journal of pharmaceutics. 2007; 343:270–276. [PubMed: 17706383]

61. Soni S, Babbar AK, Sharma RK, Maitra A. Delivery of hydrophobised 5-fluorouracil derivative to brain tissue through intravenous route using surface modified nanogels. Journal of Drug Targeting. 2006; 14:87–95. [PubMed: 16608735]

62. Bondi ML, Craparo EF, Giammona G, Drago F. Brain-targeted solid lipid nanoparticles containing riluzole: preparation, characterization and biodistribution. Nanomedicine. 2010; 5:25–32. [PubMed: 20025461]

63. Wilson B, Samanta MK, Santhi K, Kumar KP, Paramakrishnan N, Suresh B. Poly(n-butylcyanoacrylate) nanoparticles coated with polysorbate 80 for the targeted delivery of rivastigmine into the brain to treat Alzheimer's disease. Brain Research. 2008; 1200:159–168. [PubMed: 18291351]

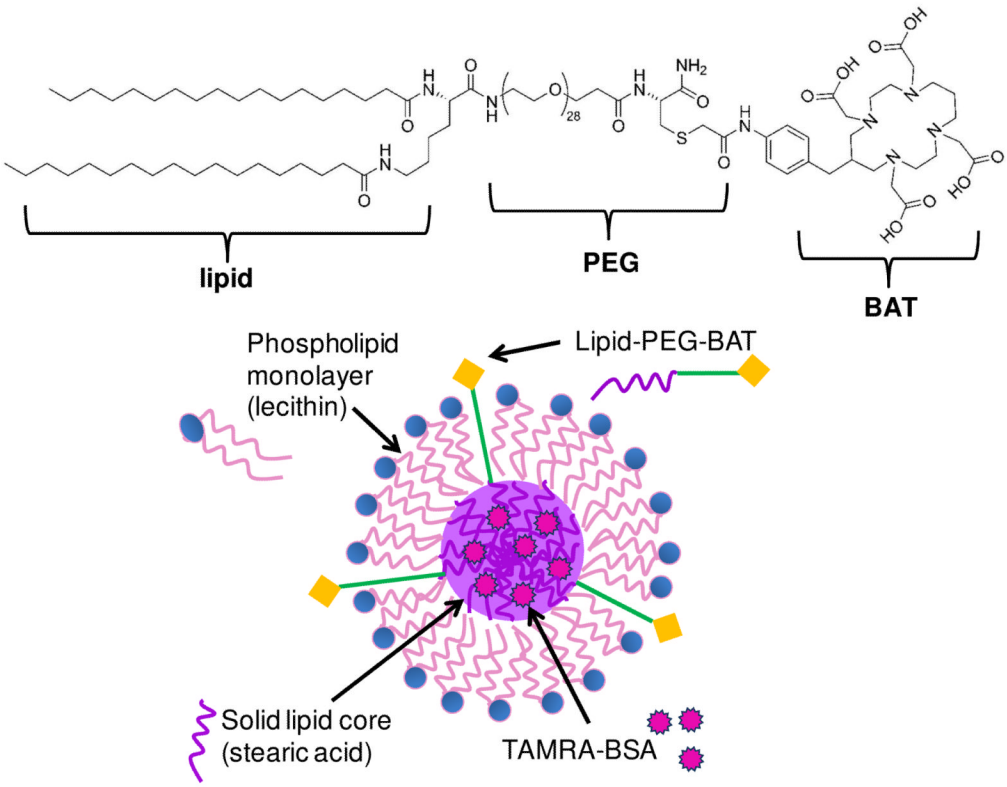

Fig. 1. Schematic of SLN-BAT

The lipid-PEG-BAT (left) molecule is incorporated into the SLN such that the stearic acid lipid tail is embedded in the stearic acid lipid core, while the PEG is associated with the lecithin monolayer, and the BAT chelator remains accessible from outside the SLN (right). We anticipate that van der Walls forces would cause the lipid portion of the lipid-PEG-BAT molecule to associate with the lipid core of the SLN and there be incorporated inside. We also anticipate that van der Walls forces would cause the hydrophilic PEG portion of the lipid-PEG-BAT to be associated with the hydrophilic headgroups of the lecithin molecule, leaving the BAT accessible on the surface of the SLN. By testing the ability for the SLNs to radiolabel ^{64}Cu, we validate the incorporation of lipid-PEG-BAT into the SLN and the accessibility of the BAT groups on the surface.

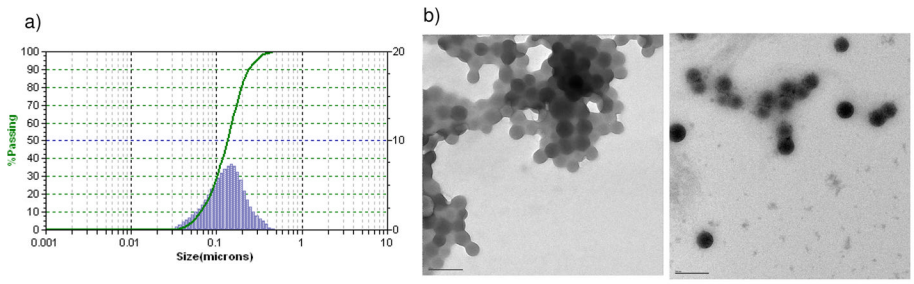

Fig. 2. Size characterization of SLNs

(a) Average Hydrodynamic diameter (145.2 ± 0.07 nm) of the optical SLNs, measured using dynamic light scattering (DLS). (b) Transmission electron microscopy (TEM) images of the 10-fold (left) and 20-fold (right) diluted SLN suspensions showing the mean dehydrated SLN diameter = 89 nm; scale bar = 100 nm.

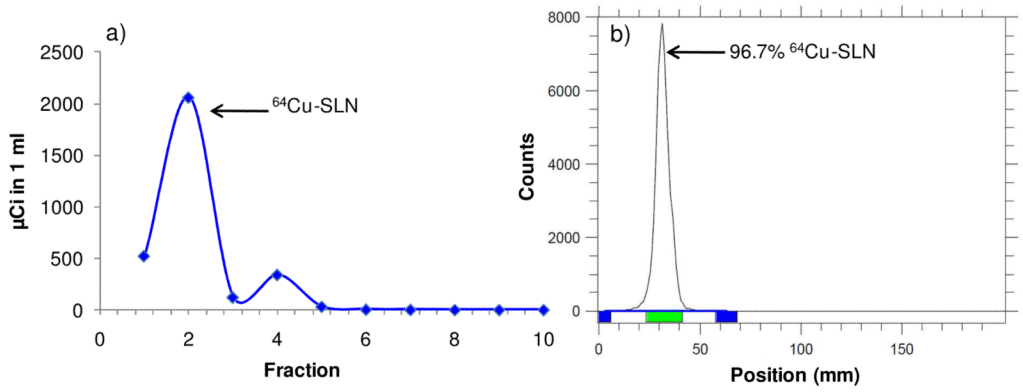

Fig. 3. Radiolabeling yield (%) and purification of SLNs

(a) Elution profiles of ^{64}Cu-SLN after incubation with $^{64}CuCl_2$ (1 hr) and EDTA (25 min) at 25°C and separation through a size-exclusion column. (b) Following purification, radio TLC of ^{64}Cu-SLN on a silica plate was developed with methanol/ammonium acetate (10%) (50:50, v/v) and recorded by a radio-TLC Imaging Scanner. Results show >95% radiolabeled nanoparticles.

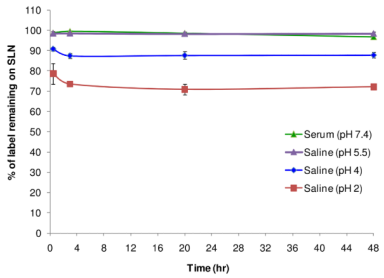

Fig. 4. Stability of SLNs

Stability of radiolabeled solid lipid nanoparticles (SLNs) over 48 hr in serum (pH 7.4), saline (pH 5.5), saline (pH 4), and saline (pH 2). Bars represent mean ± standard deviation (n = 3/group).

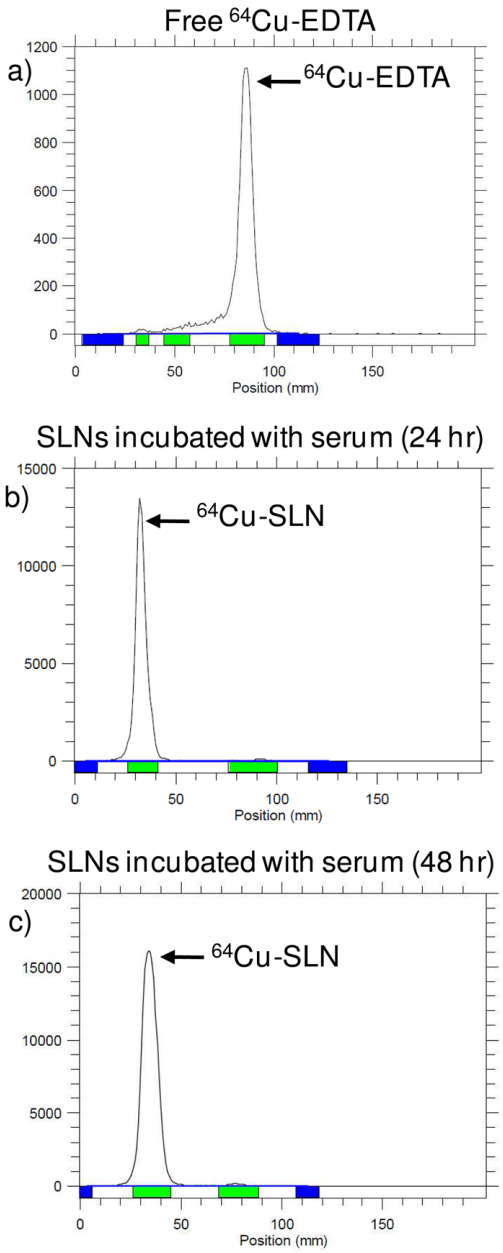

Fig. 5. Radio TLC of SLNs incubated with serum

Cu-EDTA (a) and SLNs incubated with serum at 24 (b) and 48 hr (c) were developed on a silica plate with methanol/ammonium acetate (10%) (50:50, v/v) and recorded by a radio-TLC Imaging Scanner. The absence of free ^{64}Cu-EDTA in b) and c) confirm that the ^{64}Cu-SLNs were stable in plasma after 24 and 48 hr.

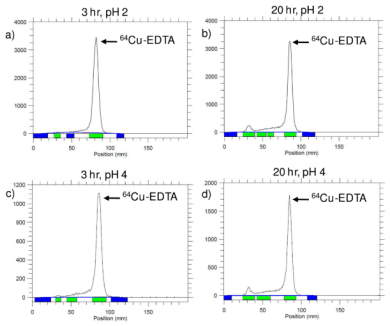

Fig. 6.

Radio TLC of supernatant resulting from centrifugation filtration of SLNs incubated with saline (pH 2) and saline (pH 4) at 3 and 20 hr. Samples were developed on a silica plate was developed with methanol/ammonium acetate (10%) (50:50, v/v) and recorded by a radio-TLC Imaging Scanner. The TLC plots confirm that the loss of radiolabel observed (Figure 4) for ^{64}Cu-SLNs incubated with saline (pH 2) and saline (pH 4) were a result of ^{64}Cu-EDTA dissociating from the particle in these extreme conditions.

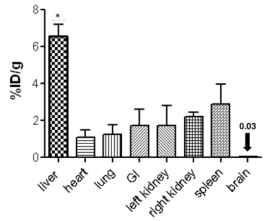

Fig. 7. Biodistribution with gamma counting

Biodistribution of ^{64}Cu-SLNs in mice at 52–55 hr post injection. Error bars represent mean ± standard deviation (n = 3). Liver activity (%ID/g) is significantly higher (p value < 0.01) than all other organs.

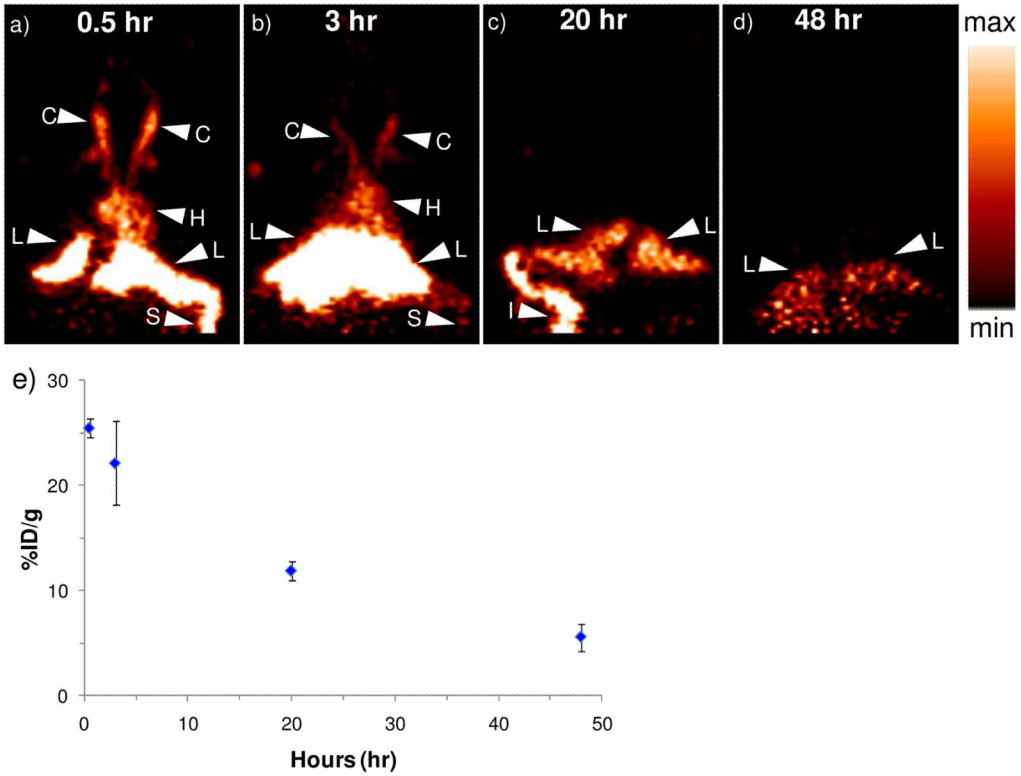

Fig. 8. Preliminary biodistribution with PET

Coronal view of a microPET image acquired at (a) 0.5-hr, (b) 3-hr, (c) 20-hr, and (d) 48-hr post i.v. injection of ^{64}Cu-SLNs. Radioactive signal is present in C = carotid, H = heart, L = liver, S = spleen, and I = intestines. A relative scale (the brightest spot is maximum) was applied for the images; e) Liver biodistribution obtained using ROI analysis on the microPET images. Error bars represent mean ± standard deviation (n = 3).

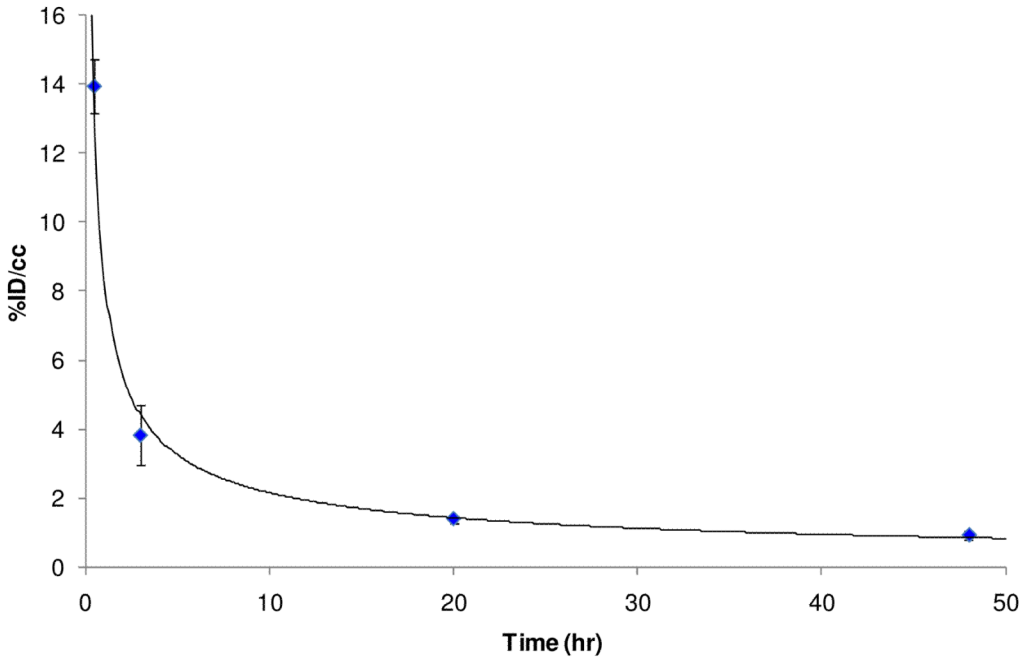

Fig. 9.

Time activity curve (TAC) of blood after bolus i.v. injection of ^{64}Cu-SLNs in mice. TACs were obtained with region-of-interest (ROI) analysis using ASIPro software and expressed as the percentage of injected dose per cubic centimeter (%ID/cc). Error bars represent mean ± standard deviation (n = 3). The monoexponential curve fit to the data was as follows: $y = 8.4363x^{-0.593}$.

Table 1

Preparation of SLN with optical cargo: W/O and W/O/W phase composition

W/O Phase		W/O/W Phase	
Materials	**Amount**	**Materials**	**Amount**
Stearic acid	67.2 mg, 0.24 mol	**Nanopure water**	158.3 mg
Lecithin	40.2 mg, 0.05 mol	**Lecithin**	8.5 mg, 0.01 mol
1-Butanol	32.6 mg, 0.44 mol	**Sodium taurodeoxycholate**	10.4 mg, 0.02 mol
BSA-TAMRA (aq)	10.2 mg, 0.0002 mol	**1-Butanol**	2.8 mg, 0.04 mol
	N/A	**W/O phase**	18.00 mg